THE OFFICIAL MAGAZINE OF THE OCEANOGRAPHY SOCIETY

Oceanography

CITATION

Hurlburt, H.E., E.J. Metzger, J. Sprintall, S.N. Riedlinger, R.A. Arnone, T. Shinoda, and X. Xu. 2011. Circulation in the Philippine Archipelago simulated by 1/12° and 1/25° Global HYCOM and EAS NCOM. *Oceanography* 24(1):28–47, doi:10.5670/oceanog.2011.02.

Circulation in the Philippine Archipelago

Simulated by 1/12° and 1/25° Global HYCOM and EAS NCOM

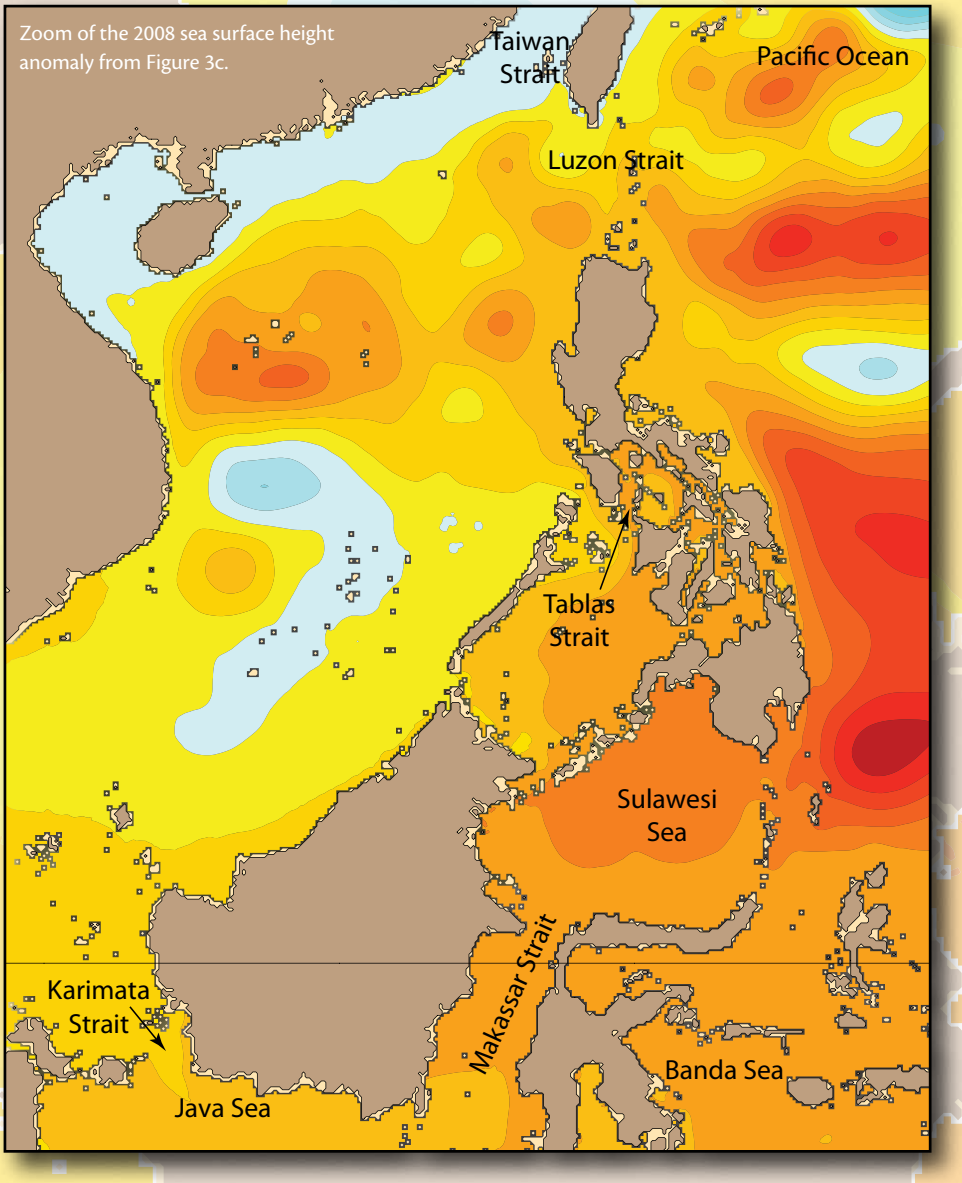

BY HARLEY E. HURLBURT, E. JOSEPH METZGER, JANET SPRINTALL, SHELLEY N. RIEDLINGER, ROBERT A. ARNONE, TOSHIAKI SHINODA, AND XIAOBIAO XU

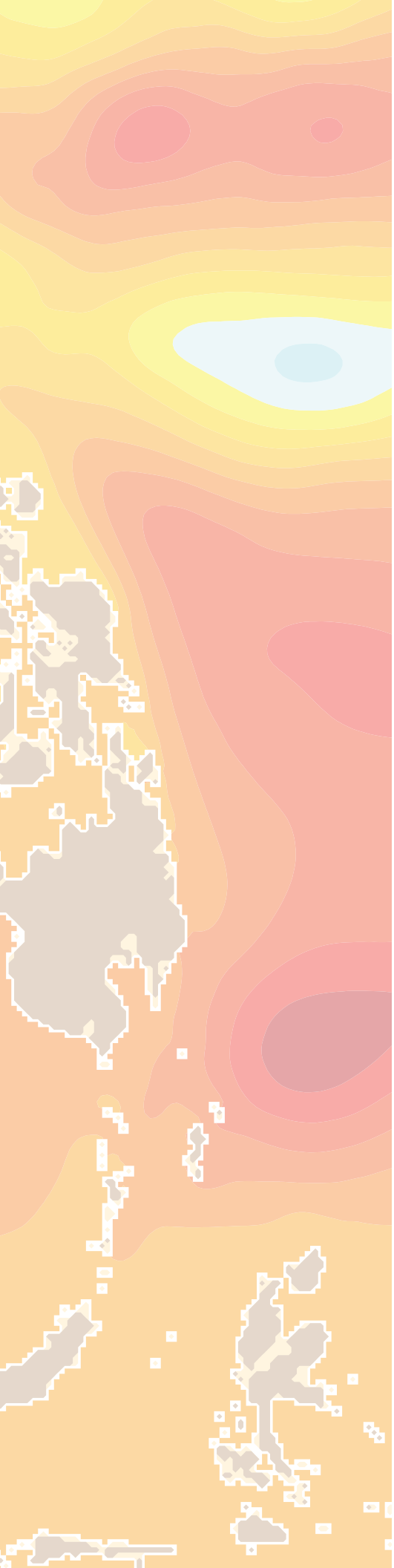

ABSTRACT. Three ocean models, 1/25° global HYbrid Coordinate Ocean Model (HYCOM), 1/12° global HYCOM, and East Asian Seas Navy Coastal Ocean Model (EAS NCOM) nested in global NCOM, were used to provide a global context for simulation of the circulation within the Philippine Archipelago as part of the Philippine Straits Dynamics Experiment (PhilEx). The Philippine Archipelago provides two significant secondary routes for both the Indonesian throughflow and the western boundary current of the Pacific northern tropical gyre. The deeper route enters the archipelago from the north through Mindoro Strait, after passing through Luzon Strait and the South China Sea. The second route enters directly from the Pacific via the shallow Surigao Strait and passes through Dipolog Strait downstream of the Bohol Sea. Both pathways exit via Sibutu Passage and the adjacent Sulu Archipelago along the southern edge of the Sulu Sea, and both are deeper than the pathway into the Indonesian Archipelago via Karimata Strait in the Java Sea. Within the Philippine Archipelago, these pathways make the dominant contribution to the mean circulation and much of its variability, while their outflow contributes to the flow through Makassar Strait, the primary conduit of the Indonesian throughflow, at all depths above the Sibutu Passage sill. Because of the narrow straits and small interior seas, the simulations are very sensitive to model resolution (4.4 km in 1/25° global HYCOM, 8.7 km in 1/12° global HYCOM, and 9.6 km in EAS NCOM in this latitude range) and to topographic errors, especially sill depths. The model simulations for 2004 and 2008 (the latter the central year of the PhilEx observational program) show extreme opposite anomalous years with anomalously strong southward Mindoro transport in 2004 and mean northward transport in 2008, but with little effect on the Surigao-Dipolog transport. Satellite altimetry verified the associated HYCOM sea surface height anomalies in the western tropical Pacific and the South China Sea during these extreme years. A 15-month (December 2007–March 2009) PhilEx mooring in Mindoro Strait measured velocity nearly top to bottom at a location close to the sill. The 1/12° global HYCOM, which showed the strongest flow above 200 m lay west of the mooring, was used to adjust a Mindoro transport estimate from the mooring data for cross-sectional distribution of the velocity, giving 0.24 Sv northward over the anomalous observational period. The results from the observational period were then used to adjust the 2004–2009 model transport, giving a mean of 0.95 Sv southward. The 1/25° global HYCOM simulated the observed four-layer flow in Dipolog Strait and the vigorous and persistent cyclonic gyre in the western Bohol Sea, observed during all four PhilEx cruises and in ocean color imagery. This gyre was poorly simulated by the two models with ~ 9 km resolution. Finally, a 1/12° global HYCOM simulation with tides generated the hydrostatic aspect of the internal tides within the Philippine Archipelago, including a strong internal tidal beam initiated at Sibutu Passage and observed crossing the Sulu Sea.

INTRODUCTION

In the Philippine Straits Dynamics Experiment (PhilEx), global ocean models with resolutions as fine as 1/25° (4.4 km over the latitude range 0–11° and finer at higher latitudes) are used to investigate the circulation within the Philippine Archipelago in a global context, both spatially and temporally. These models also provide boundary conditions for nested regional models (e.g., Han et al., 2009; Arango et al., 2011; Lermusiaux et al., 2011), with nests as fine as ~ 1 km feasible with boundary conditions directly from the 1/25° global model. A global context is essential because the Philippines provide secondary pathways for the Pacific to Indian Ocean throughflow (Ilahude and Gordon, 1996; Metzger et al., 2010) and secondary routes to close the northern tropical gyre, which spans the North Pacific between the North Equatorial Countercurrent (NECC) on the south and the North Equatorial Current (NEC) on the north. This gyre is bounded on the west by the southward Mindanao Current and by secondary routes through the Philippine Archipelago (Metzger and Hurlburt, 1996). Metzger et al. (2010) show outflow from Sibutu Passage feeding both into the Indonesian throughflow via Makassar Strait and into the Pacific northern tropical gyre via the NECC in a 1/12° global simulation (their Figure 9a). The deepest of the secondary routes surrounds most of the archipelago via Luzon Strait to the north and Mindoro Strait and Sibutu Passage to the west. Within the archipelago, these secondary pathways constitute the dominant contribution to the mean circulation and are responsible for much of its variability. Han et al. (2009) discuss the impacts of remote and local forcing on the seasonal variability.

Realistic modeling of the circulation within the Philippine Archipelago is an extreme challenge for a global ocean model due to the numerous narrow straits and small interior seas. Accurate modeling of flows through straits requires accurate modeling of the effects of hydraulic control and appropriate partitioning between geostrophic and hydraulic control. In a complex archipelago like the Philippines, the challenge is increased by the need to correctly partition the flow among numerous alternative routes throughout the archipelago. These issues make simulations in this region particularly sensitive to model resolution, to errors in model topography and atmospheric forcing, and to model numerics and physics. Thus, the Philippine Archipelago poses severe tests for the models, tests that are performed using data from the PhilEx field program and other sources. In turn, the models are used to help interpret the data and their ability to measure observed phenomena, to place the observations within the context of the larger-scale circulation and its temporal variability, and to help understand the dynamics of observed phenomena.

OCEAN MODEL EXPERIMENTS

Philippine Archipelago circulation is investigated using 1/12° and 1/25° global simulations by the HYbrid Coordinate Ocean Model (HYCOM; Bleck, 2002) and data assimilative nowcasts by the East Asian Seas Navy Coastal Ocean Model (EAS NCOM) with tides. EAS NCOM (9.6-km resolution at 10° latitude) has been running in real time since October 2003, and is nested in global NCOM (Barron et al., 2006), which has 19.2-km resolution at 10° latitude. Global NCOM is an operational forecast model of the US Navy (without tides) that assimilates a wide variety of ocean data. Table 1 summarizes the characteristics of the HYCOM simulations and EAS NCOM. The global HYCOM simulations were spun up for 10 years after initialization from the Generalized Digital Environmental Model 3 (GDEM3) hydrographic climatology (Carnes, 2009) and forced with an atmospheric climatology derived from the European Centre for Medium-Range Weather Forecasts (ECMWF) 40-year reanalysis (ERA-40) (Kållberg et al., 2004; HYCOM Exps. 1/12°–18.0 and 1/25°–4.0). The simulations were then continued

Harley E. Hurlburt *(harley.hurlburt@nrlssc.navy.mil) is Senior Scientist for Ocean Modeling and Prediction, Oceanography Division, Naval Research Laboratory (NRL), Stennis Space Center, MS, USA.* **E. Joseph Metzger** *is Meteorologist, Oceanography Division, NRL, Stennis Space Center, MS, USA.* **Janet Sprintall** *is Research Oceanographer, Climate, Atmospheric Science, and Physical Oceanography Division, Scripps Institution of Oceanography, La Jolla, CA, USA.* **Shelley N. Riedlinger** *is Oceanographer, Oceanography Division, NRL, Stennis Space Center, MS, USA.* **Robert A. Arnone** *is Head, Ocean Sciences Branch, Oceanography Division, NRL, Stennis Space Center, MS, USA.* **Toshiaki Shinoda** *is Oceanographer, Oceanography Division, NRL, Stennis Space Center, MS, USA.* **Xiaobiao Xu** *is Research Scientist, Department of Marine Sciences, University of Southern Mississippi, Stennis Space Center, MS, USA.*

Table 1. Ocean model experiments

Ocean Model	Experiment Number[a]	Horizontal Resolution at 10°N[a]	Vertical Resolution[b]	Atmospheric Forcing[c]	Years Used	Tides	Data Assimilation
1/12° global HYCOM	18.0	8.7 km	32 coordinate surfaces	ECMWF/ QuikSCAT	5–10	No	No
1/12° global HYCOM	18.2	8.7 km	32 coordinate surfaces	NOGAPS/ ECMWF/ QuikSCAT	2003–2010	No	No
1/25° global HYCOM	4.0	4.4 km	32 coordinate surfaces	ECMWF/ QuikSCAT	5–10	No	No
1/25° global HYCOM	4.1&2[d]	4.4 km	32 coordinate surfaces	NOGAPS/ ECMWF/ QuikSCAT	2004–2009	No	No
1/12° global HYCOM	14.1&2[e]	8.7 km	32 coordinate surfaces	NOGAPS/ ECMWF	2004–2008	Yes[f]	No
EAS NCOM	—	9.6 km	40 levels	NOGAPS	2004–2009	Yes[f]	Yes

[a] Resolution for each prognostic variable. For HYCOM the nominal resolution in degrees is the equatorial resolution, which is .08° ≈ 1/12° and .04° = 1/25°. The HYCOM experiments are from the GLBa series and all experiments use topography based on DBDB2 by D.S. Ko (see http://www7320.nrlssc.navy.mil/DBDB2_WWW).
[b] HYCOM has a hybrid isopycnal/pressure ≈ depth/terrain-following vertical coordinate. NCOM has depth coordinates with terrain-following at depths shallower than 137 m.
[c] See text.
[d] Exp. 4.2 is a 2005–2009 extension of 4.1 with changes in some frictional parameter values in a remote area.
[e] Exp. 14.2 is a one-month (May 2004) repeat of 14.1 with global hourly three-dimensional output.
[f] Eight tidal constituents.

interannually using archived operational forcing from the Navy Operational Global Atmospheric Prediction System (NOGAPS) (Rosmond et al., 2002), but with the long-term annual mean replaced by the long-term mean from ERA-40 (Exp. 1/12°–18.2 initialized from 18.0 and Exp. 1/25°–4.1&2 from 4.0 [Table 1]). In most of the experiments, wind speed was corrected using a monthly climatology from the QuikSCAT scatterometer (Kara et al., 2009). Model experiment 1/12° global HYCOM-14.1&.2 is the world's first eddy-resolving global ocean simulation that includes both the atmospherically forced ocean circulation and tides (Arbic et al., 2010). The 1/25° global HYCOM began running on January 12, 2009, and has the highest resolution used thus far in a global ocean general circulation model (OGCM) with thermohaline dynamics and more than a few layers in the vertical.

HYCOM is a community ocean model (http://www.hycom.org) with a generalized vertical coordinate because no single coordinate is optimal everywhere in the global ocean. Isopycnal (density-tracking) layers are best in the deep stratified ocean, pressure levels (nearly fixed depths) provide high vertical resolution in the mixed layer, and σ-levels (terrain-following) are often the best choice in coastal regions (Chassignet et al., 2003). The generalized vertical coordinate in HYCOM allows a combination of all three types (and others), and the optimal distribution is chosen dynamically at every time step using the layered continuity equation. NCOM is a depth coordinate ocean model with a terrain-following coordinate at depths shallower than 137 m.

MEAN CIRCULATION SIMULATED BY 1/12° AND 1/25° GLOBAL HYCOM AND THE IMPACT OF TOPOGRAPHIC ERRORS

Figure 1a,b is a comparison of the mean currents at 20-m depth and strait transports from 1/12° global HYCOM-18.2 with those from 1/25° global HYCOM-4.1&2, and Figure 1c,d is a comparison of their respective topographies and sill depths. Because the 1/12° topography was derived from the 1/25°, they demonstrate close agreement in deep water, although numerous hand

edits were subsequently applied to the 1/12° topography (Metzger et al., 2010), mainly in shallow water and to correct sill depths. Edits to the 1/25° topography were done later, and fewer were made. In Figure 1, some of the sill depths in the two models are in good agreement, but there are substantial differences in the Dipolog Strait, Surigao Strait, and Sibutu Passage sill depths and in the topography along the entire southern archipelago of the Sulu Sea. The topography of this archipelago is not adequately known, nor are the sill depths of San Bernardino and Surigao straits.

Figure 1a,b depicts two main routes for flow through the Philippine Archipelago: a deeper pathway from the South China Sea via Mindoro Strait to outflow through Sibutu Passage, and a shallow pathway from the Pacific via Surigao and Dipolog straits, also to outflow through Sibutu Passage. With the resolution increase from 1/12° to 1/25°, a very large increase in transport is seen through Mindoro Strait (where the topography and sills depths are in good agreement) and through Sibutu Passage (Figure 1a,b). In contrast, a relatively modest increase occurs through Surigao and Dipolog (despite the very large Dipolog sill depth error and a 1.8-fold deeper Surigao sill depth in 1/25° global HYCOM). These results indicate that the mean transport of the Mindoro to Sibutu pathway is largely constrained by the outflow through Sibutu Passage, while the transport of the shallower pathway is mainly determined by the inflow through Surigao. Thus, it is most critical to improve the topography and sill depths of Sibutu

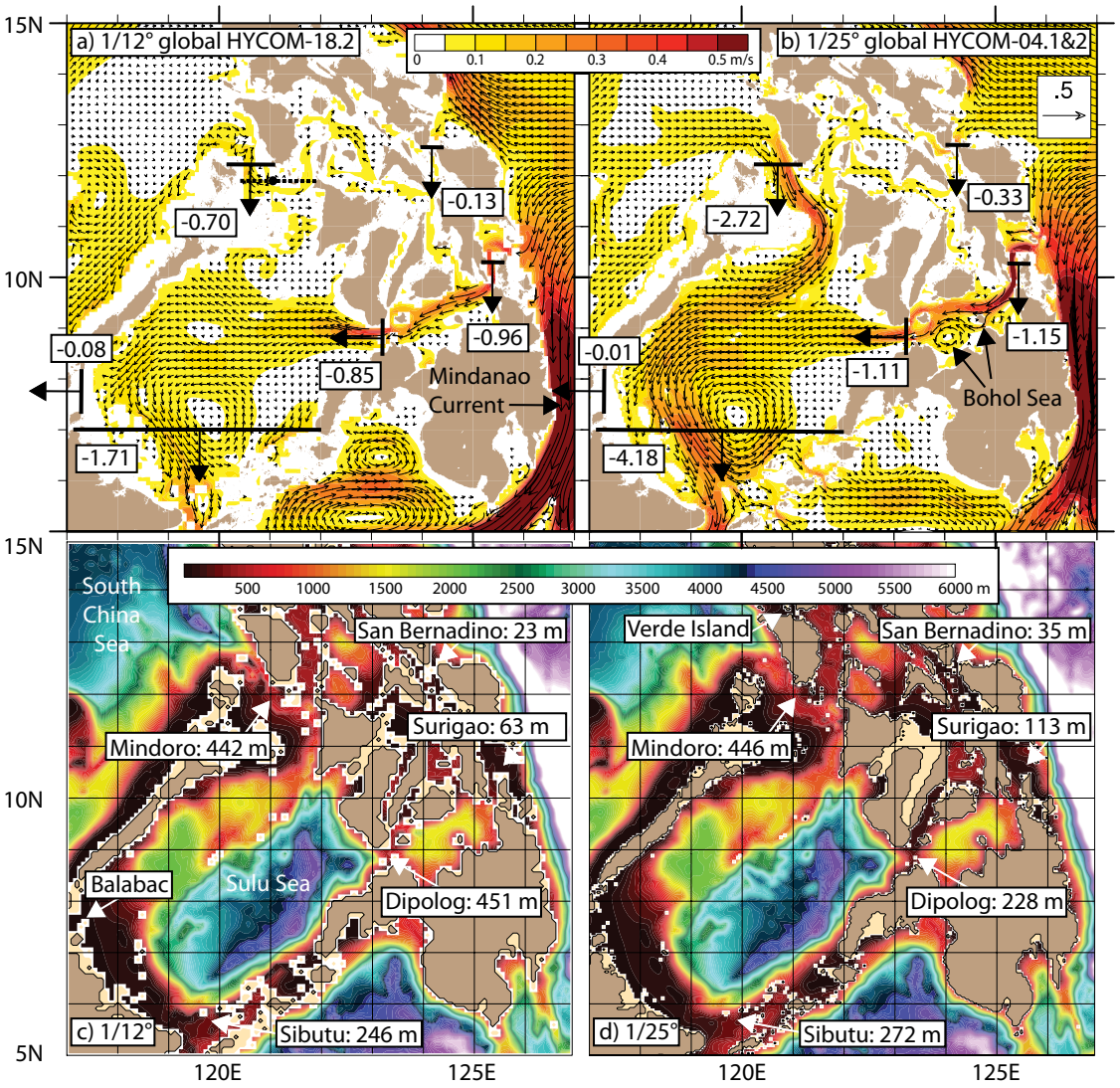

Figure 1. (a,b) Mean currents (m s^{-1}) overlaid on speed (in color) at 20-m depth in and around the Philippine seas from (a) 1/12° global HYbrid Coordinate Ocean Model (HYCOM)-18.2 and (b) 1/25° global HYCOM-4.1&2. See Table 1 and related discussion in the "Ocean Model Experiments" section. The 2004–2009 mean transport through straits labeled on (a,b) (in Sv = 10^6 m^3 s^{-1}) is given in boxes with negative values for southward and westward, as indicated by the attached arrows. The speed contour is 0.05 m s^{-1} and the reference vector is 0.5 m s^{-1} (upper right in panel b). Every second (fourth) vector is plotted in panel a (b). (c,d) Bottom topography for (a) 1/12° global HYCOM and (b) 1/25° global HYCOM with sill depths given for key straits.

Passage and the adjacent passages through the Sulu Archipelago. There is also a 2.5-fold increase in transport through the very shallow San Bernardino Strait. The increased transport through San Bernardino has a marked impact on the mean flow through the interior passages of the Philippines between Surigao Strait and Tablas Strait, which lies just east of Mindoro (Figure 2a). In 1/12° (1/25°) global HYCOM, there is a net transport of 0.11 Sv (0.04 Sv) from Surigao to Tablas versus 0.13 Sv (0.33 Sv) from San Bernardino to Tablas.

In 1/12° global HYCOM, both of the straits bordering the Pacific, San Bernardino and Surigao, are characterized by choke points that are one grid point wide and one grid point long, so why the large difference in the transports (Figure 1a)? An explanation based solely on the difference in sill depths (Figure 1c) is not sufficient. A model by Mattsson (1995; a barotropic version of Equation A5 in Metzger and Hurlburt, 1996) relates transport through a strait (Q) to the upstream-downstream change in sea surface height (ΔSSH) based on a combination of geostrophic and hydraulic control, the latter including contributions from Bernoulli setdown and bottom friction. The relationship between Q and ΔSSH is given entirely in terms of physical and geometric parameters. The mean 2004–2009 ΔSSH is 8 cm for San Bernardino and 6 cm for Surigao. Using the sill depth and a bottom friction coefficient of $C_b = 2.5 \times 10^{-3}$ gives close agreement at San Bernardino, but not at Surigao. At San Bernardino, the depth in the choke point is 29 m and the sill is one grid point upstream. In

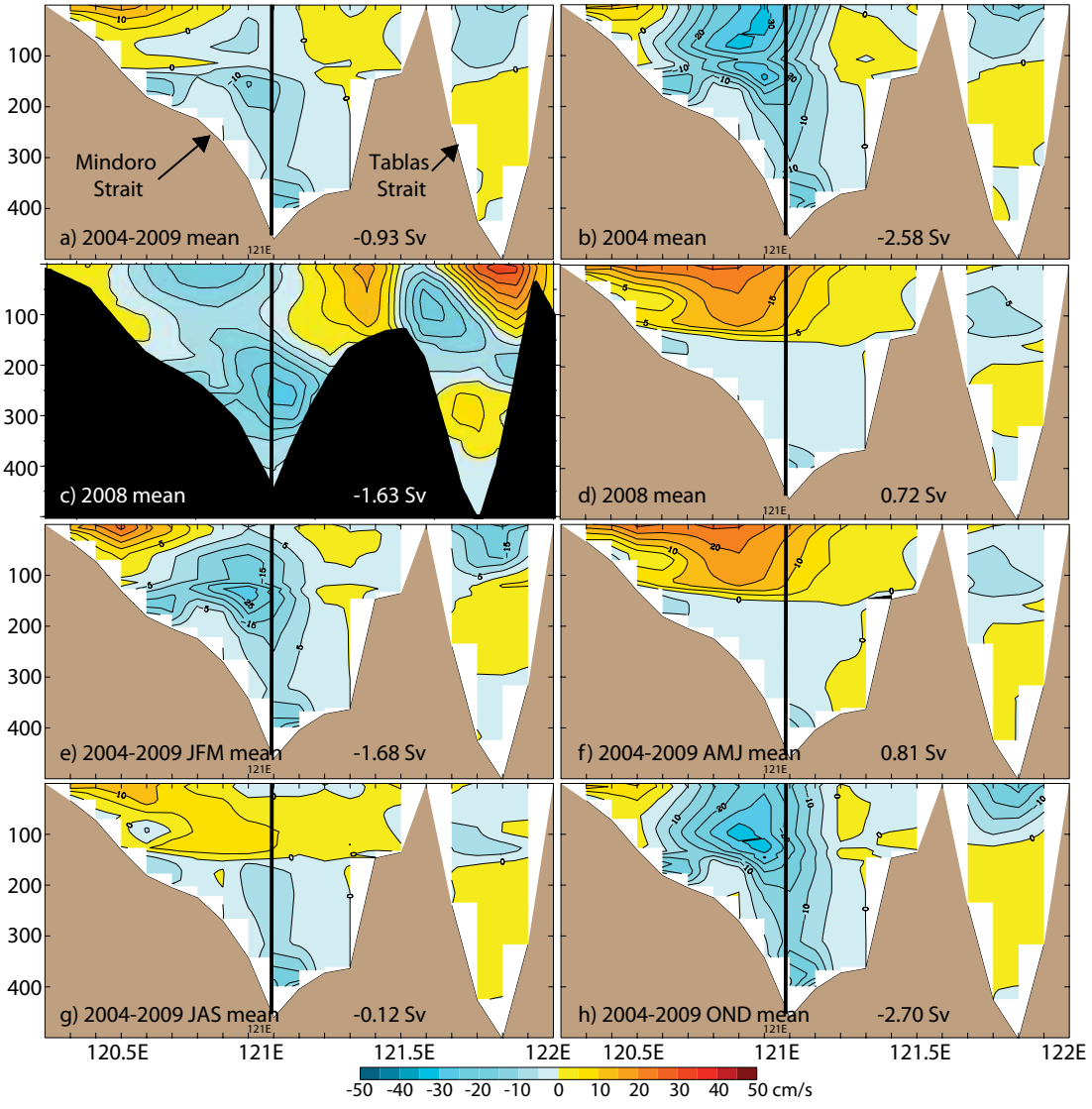

Figure 2. (a–d) Mean meridional velocity cross sections at 11°54′N, the latitude of the PhilEx Mindoro mooring (marked with a vertical line on the cross sections), near the location where Mindoro and Tablas straits join (dashed line on Figure 1a). The labeled transports are for the entire cross section and all means are over the time period labeled on the figure panel. (e–h) Seasonal means over 2004–2009 for JFM (January–March, winter), AMJ (spring), JAS (summer), and OND (fall). All are from 1/12° global HYCOM-18.2, except (c) is from East Asian Seas Navy Coastal Ocean Model (EAS NCOM.)

contrast, at Surigao the depth in the choke point is 987 m and located at the western exit point, while the sill is near the eastern entrance in a relatively broad area of similar depths. At the Surigao exit point, the current has extended downward through the mixed layer and into the upper thermocline (~ 120-m deep). When a depth of 120 m and $C_b = 0$ is used at the choke point in Surigao, the ΔSSH predicted by Equation A5 is in close agreement with the 6 cm seen in the model, supporting the earlier indication that Surigao controls the transport of the Surigao-Dipolog-Sibutu route for flow through the Philippine Archipelago. This article contains all the information used in the barotropic version of Equation A5 in Metzger and Hurlburt (1996). Additional factors also have an impact on flow through the straits, such as differences in topographic configuration, increased numerical accuracy at higher resolution, effects of tides on bottom friction, and reduced horizontal friction with increased resolution (because some friction parameters scale with model resolution).

The outflow from the interannual HYCOM simulations, discussed above, contributes to the transport through Makassar Strait at all depths above the Sibutu Passage sill. However, despite the differences in Sibutu Passage transport in these simulations, the transport through Makassar Strait is nearly the same (Table 2). These results imply either a variation in the contribution from the Mindanao Current (see Figure 1a)—the case in these simulations—or a direct contribution from Sibutu Passage to the NECC, as seen in the results of Metzger et al. (2010). The impact on the contribution from the Mindanao Current, while Makassar transport remains unchanged, suggests an indirect contribution to the NECC, as demonstrated by Metzger and Hurlburt (1996, their Plate 2) and in the next section. Additionally, Metzger and Hurlburt (1996, their Table 3b) performed a set of eight global ocean

Table 2. Transports (Sv) through straits, model 2004–2009 vs. observed

Strait	Transect Orientation[a]	EAS NCOM[b]	1/12° HYCOM 18.2	1/25° HYCOM 4.1 and 4.2	Observed Transport
Mindoro	EW	−2.85	−0.70	−2.72	−0.95[c]
Mindoro overflow[d]	EW	−0.08	−0.22	−0.21	−0.28[c]
San Bernardino	EW	−0.18	−0.13	−0.33	—
Surigao	EW	−1.45	−0.96	−1.15	—
Sibutu	EW	−4.81	−1.71	−4.18	—
Tablas	EW	−0.51	−0.23	−0.36	—
Dipolog	NS	−1.10	−0.85	−1.11	—
Verde Island	NS	−0.01	0.0	0.01	—
Balabac	NS	0.19	−0.08	−0.01	—
Luzon	NS	−4.92	−2.89	−5.17	−3.0[e]
Taiwan	EW	1.40	1.60	1.74	1.8[f]
Karimata	EW	−0.50	−0.54	−0.61	−0.8[g]
Makassar	EW	−12.26	−14.00	−13.70	−11.6[h]

[a] The transect orientation is either east-west (EW) or north-south (NS), and the sign convention is positive northward/eastward and negative southward/westward.
[b] The EAS NCOM mean transport is computed over the period February 2004 through December 2009.
[c] See Table 3.
[d] Transport below 350 m.
[e] Qu (2000), based on hydrographic data down to 400 db.
[f] Wang et al. (2003), based on 2.5 years (1999–2001) of shipboard acoustic Doppler current profiler data.
[g] Fang et al. (2010), extrapolated estimate based on 11 months (December 4, 2007–November 1, 2008) of mooring data.
[h] Gordon et al. (2008), based on three years (2004–2006) of mooring data.

simulations with a wide range of transports (0 to 12 Sv) through Sibutu Passage and through Karimata Strait in the western Java Sea. In their simulations, the transport of Pacific Ocean to Indian Ocean throughflow was very insensitive to the transports through these straits, and the Makassar transport was insensitive to Sibutu Passage transport. All of their simulations used the same monthly global wind stress climatology, except that the wind stress was zeroed over the Philippine Archipelago, the South China Sea, and northeast of Luzon Strait in two of the simulations.

MINDORO STRAIT: THE DEEPEST CONNECTION TO THE PHILIPPINE SEAS

Mindoro Strait is the deepest passage connecting the interior seas of the Philippine Archipelago to the large-scale ocean circulation (Figure 1) and is predominantly an inflow pathway. Figure 2 depicts cross sections of meridional velocity through Mindoro and Tablas straits near the location where they join (section marked by the dashed line on Figure 1a). The latitude of the cross section coincides with that of a PhilEx mooring near the Mindoro sill, which is depicted by a vertical line in Figure 2. Strong seasonal and interannual variabilities of comparable amplitude are evident in the meridional velocity, with variability seen at all depths, but with the largest variability located in and above the thermocline (Figure 2). The extreme opposite transports during the seasonal cycle occur during the monsoon transition seasons with the largest southward transport occurring during the boreal fall onset of the northeast monsoon (Figure 2h) and mean northward transport during the spring transition to the southwest monsoon (Figure 2f). Weaker southward transport occurs during the winter peak of the northeast monsoon (Figure 2e), and mean transport is very low during the summer southwest monsoon (Figure 2g), similar to the seasonal cycle reported by Han et al. (2009), who focused on the upper 40 m and found that, below the Ekman layer, the seasonal cycle of the Mindoro-Sibutu pathway is driven largely by remote forcing.

> "REALISTIC MODELING OF THE CIRCULATION WITHIN THE PHILIPPINE ARCHIPELAGO IS AN EXTREME CHALLENGE FOR A GLOBAL OCEAN MODEL DUE TO THE NUMEROUS NARROW STRAITS AND SMALL INTERIOR SEAS."

The central year for PhilEx measurements was 2008, but in 1/12° global HYCOM-18.2, 2008 is a very anomalous year (Figure 2d) with flow through Mindoro Strait that is much like the spring mean (Figure 2f), including similar mean northward transport through Mindoro plus Tablas. In contrast, 2004 is an extreme opposite anomalous year (Figure 2b), much like the fall mean (Figure 2h), the season with the largest southward transport. In the model, the periods of the anomalies are well captured by the two calendar years. Neither year is a traditional El Niño or La Niña year based on the Japan Meteorological Agency (JMA) index, which has been a particularly sensitive indicator of past La Niña events (Hanley et al., 2003). The National Climatic Data Center (http://www.ncdc.noaa.gov) shows a positive Southern Oscillation Index during nearly all of 2008 (an indication of La Niña), but the NOAA Climate Prediction Center (http://www.cpc.noaa.gov) reported La Niña conditions only from late 2007 to May 2008. However, 2004 has been identified as an El Niño Modoki (pseudo-El Niño) year, where the primary warm sea surface temperature (SST) anomaly is located in the central equatorial Pacific, flanked by cool anomalies at the eastern and western ends of the tropical Pacific (Ashok et al., 2007).

Figure 3 presents 2004 and 2008 comparisons between 1/12° global HYCOM-18.2 sea surface height (SSH) anomalies and those observed by satellite altimetry (on a 1° grid from Aviso, 2010). Both the model and the altimetry show the opposite anomalies of 2004 and 2008 spanning the domain depicted in Figure 3, essentially a strengthening (weakening) of the northern tropical gyre in the western Pacific in 2004 (2008), but with the anomalies extending northward to the entrance of Luzon Strait into the South

China Sea, well north of the northern tropical gyre and the North Equatorial Current, the strength of which is not substantially impacted by the anomalies. A strong gradient in SSH anomaly is seen at the northern edge, part of which extends into the South China Sea and the Philippine Archipelago. Associated with the gradient in SSH anomaly is an anomaly in Luzon Strait transport and downstream, a transport anomaly entering the Philippine Archipelago via Mindoro Strait. The 2004 anomaly increases the southward transport entering the Philippine Archipelago through Mindoro from the 2004–2009 mean of 0.70 Sv to 2.41 Sv and the southward transport exiting through Sibutu Passage from 1.71 to 3.39 Sv. The increases are 1.71 Sv through Mindoro and 1.68 Sv through Sibutu. The Sibutu outflow transport minus the Mindoro inflow gives the combined contribution to Sibutu Passage outflow from other straits, which is 1.01 Sv in the 2004–2009 mean and 0.98 Sv in the 2004 mean. Thus, the combined contribution to the 2004 Sibutu outflow anomaly from the other straits (labeled on Figure 1) is minimal. The largest of these contributions to Sibutu Passage transport is the direct inflow from the Mindanao Current through Surigao Strait, which has large seasonal variability but little interannual variability in the yearly means. The transport through Mindoro Strait in 2008 demonstrates a 1.66 Sv anomaly in the opposite direction from 2004 (from 0.70 Sv southward in the mean to 0.96 Sv northward). Since Sibutu Passage transport changes from a mean of 1.71 Sv southward to 0.07 Sv northward in 2008, the outflow through Mindoro is fed largely by inflow through Surigao Strait via Dipolog Strait. Consistent with these results, the SSH at the two ends of Surigao Strait rises or falls in tandem by 5–6 cm from the 2004–2009 mean during each of the anomalous years, and the upstream-downstream ΔSSH values for the mean and the two anomalous years are the same within 1 cm; the situation is similar for San Bernardino Strait.

During PhilEx, a 15-month time series of velocity versus depth was obtained from the mooring in Mindoro Strait. The measurements cover nearly the full water column in the deepest part of the strait near the sill (vertical lines in Figure 2). These measurements allow the first estimate of transport through Mindoro Strait based on in situ observations. Because there was only one mooring in the strait, results from 1/12° global HYCOM-18.2 are used in combination with the data to better include the impact of the cross-strait flow structure. Additionally, the model

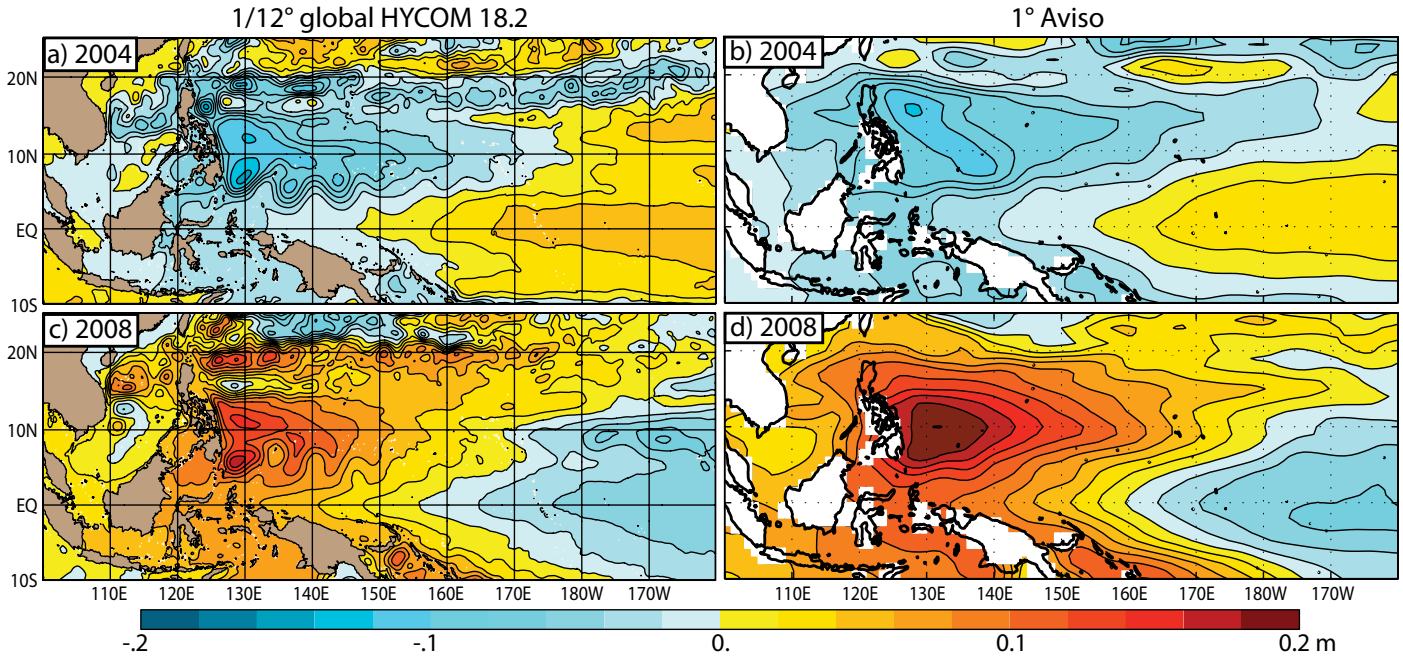

Figure 3. 2004 (a,b) and 2008 (c,d) mean sea surface height (SSH) anomalies from (a,c) 1/12° global HYCOM-18.2 with respect to a 2004–2009 mean and (b,d) 1° Aviso analyses of altimeter data with respect to a 2002–2008 mean. The contour interval is 0.02 m.

results allow an extension of the mean transport estimate obtained over the highly anomalous PhilEx time period, centered on 2008, to a more representative, longer mean over 2004–2009.

Figure 4 presents comparisons between the meridional velocity measurements and transports from the mooring and HYCOM-18.2. Figure 4a,b is a direct comparison of daily-averaged velocity versus depth over the December 22, 2007 to March 18, 2009 time period of the observations, and Figure 4c shows the mean and variability versus depth. Depiction of the two time series versus depth reveals very similar vertical structure and temporal variability, including individual events such as the upward-propagating northward anomaly in early 2008. The largest seasonal variability is seen in and

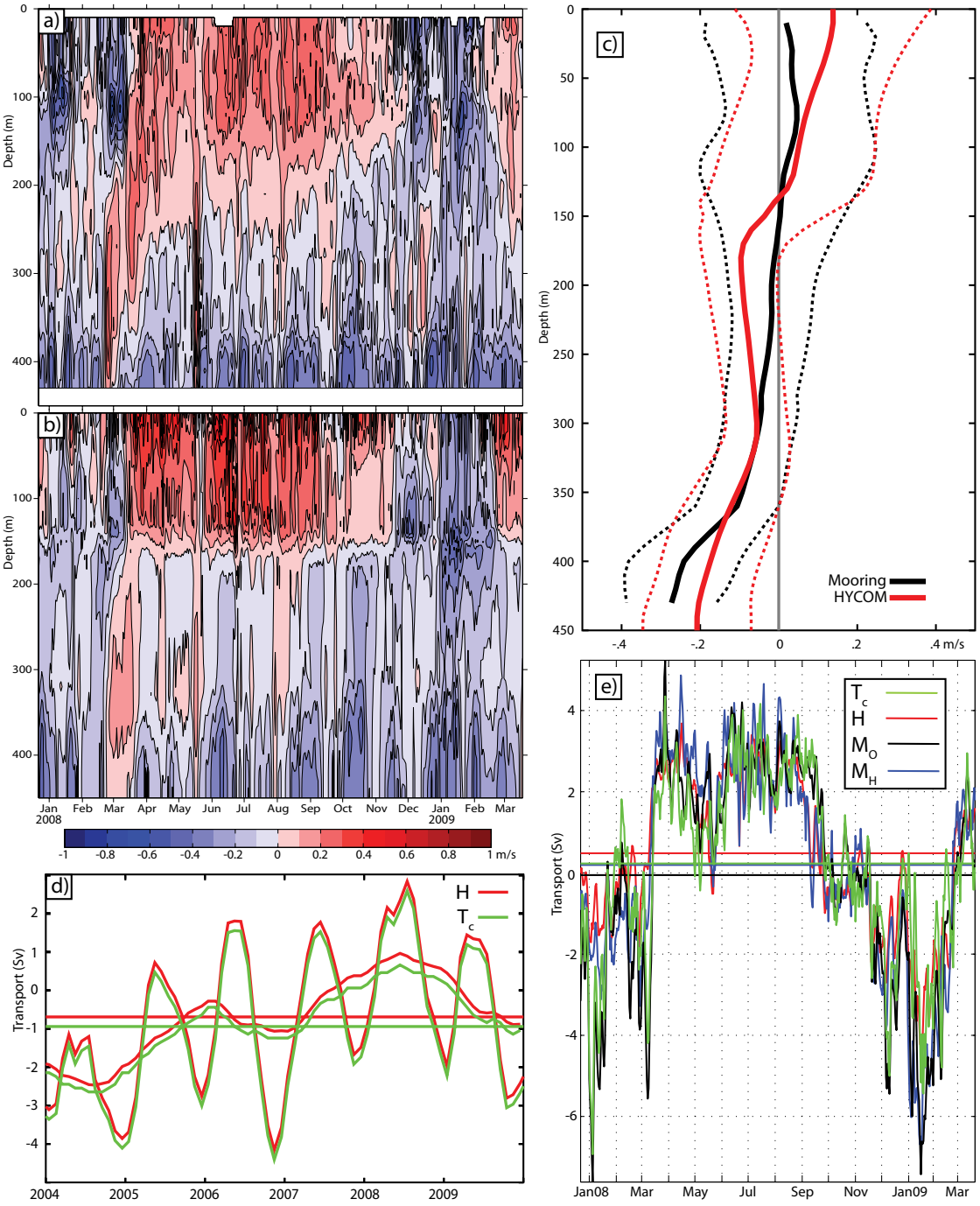

Figure 4. Mindoro Strait comparisons of daily mean meridional velocity versus depth (negative southward) over the observational period with dates labeled at the beginning of each month or year, from (a) the mooring and (b) 1/12° global HYCOM-18.2 (in m s^{-1} with a 0.1 m s^{-1} contour interval). (c) Mooring and model means (solid lines) and standard deviations (dashed) of meridional velocity component versus depth. Transport (in Sv) versus time over (d) 2004–2009 (monthly means with a 1-2-1 filter, one-year running means, and 2004–2009 mean transports) from (H) (red) 1/12° global HYCOM-18.2 and (T_c) (green) combined mooring and 1/12° HYCOM-18.2 estimates and (e) the December 22, 2007–March 18, 2009 period of the observations. Daily and observing period mean transports M_o (black) are estimated from the mooring alone, M_H (blue) from a collocated HYCOM-18.2 mooring, H (red) from HYCOM-18.2, and T_c (green), from mooring and HYCOM-18.2 combined. See Table 3 and related discussion.

above the thermocline (top ~ 140 m) with northward flow except from mid-November to mid-March, a longer period of northward flow than in other years, based on the Mindoro transport time series in Figure 4d. A sharper thermocline is seen in the model. Below the thermocline, the flow is largely southward and dominated by the event time scale. The stronger bottom-trapped southward flow depicts the sill overflow. In the mean (Figure 4c), both the model and observations show northward flow above ~ 140 m, more strongly northward in the model. The bottom-trapped southward flow is stronger in the observations than in the model simulation, which does not include tides. The vertical means are southward and in close agreement, 4.7 cm s^{-1} observed versus 4.4 cm s^{-1} in the model simulation. Both the model and observations demonstrate enhanced variability just above the thermocline.

ESTIMATION OF MINDORO STRAIT TRANSPORT

Table 3 provides Mindoro Strait transport estimates, Figure 4e presents daily transport time series over the period of the observations, and Figure 4d shows interannual time series. Transport estimates based on the vertical profiles of velocity from the observations (M_o in Table 3) and from 1/12° global HYCOM-18.2 (M_H) were obtained by assuming that the observed velocity at the mooring location is representative of the flow over half the channel width (centered near the mooring) and tapers to zero at the side walls, using the SRTM30_PLUS topography (Becker et al., 2009) with the mooring observations and the HYCOM topography with the model mooring. Over the deployment time period, the mooring data are dominated by stronger southward flows in the intermediate and overflow depths, so the total mooring transport is M_o = 0.055 Sv southward compared to M_H = 0.20 Sv northward in the 1/12° global HYCOM-18.2 simulation (Table 3). However, in the models and in repeat acoustic Doppler current profiler (ADCP) transects across the strait (Gordon et al., 2011), the strongest flow occurs west of the mooring location (e.g., Figure 2). Thus, assuming the single mooring velocity is representative across half the strait width may not be correct. Hence, the observation-based estimate (M_o) was adjusted using the difference between the HYCOM-18.2 full transect estimate (H) with model cross-passage velocity structure, and the HYCOM-18.2 mooring estimate (M_H), both over the observational period. This results in a combined estimate using observations and the model of $T_c = M_o + (H - M_H)$ = 0.24 Sv northward over the December 22, 2007–March 18, 2009 time span of the observations (Table 3). As evident in the velocity fields (Figure 4a,b), high variability is found on every time scale resolved in the transport time series of both the observed and model estimates (Figure 4e). All estimates give northward transport from mid March through October 2008 (Figure 4e). For the 2004–2009 transport estimate ($\overline{T_c}$ = 0.95 Sv southward), it was assumed that the difference between the observations and the model ($M_o - M_H$) remained the same as found during the observational deployment period, because a linear regression analysis between H and ($M_o - M_H$) showed no relationship. The resulting interannual transport time series clearly shows opposite transport anomalies in 2004 and

Table 3. Mindoro Strait mean transport estimates

Transport Estimate Source	Symbol	Total Transport Estimate (Sv)	Overflow[a] Transport Estimate (Sv)
Estimates over the time period of the observations (December 2007–March 2009)			
Mooring alone	M_o	−0.055	−0.24
Collocated HYCOM-18.2 mooring	M_H	0.20	−0.14
1/12° global HYCOM-18.2	H	0.49	−0.18
Combined mooring/HYCOM-18.2	T_c	0.24	—[b]
Estimates over 2004–2009			
1/12° global HYCOM-18.2	$\overline{H}$	−0.70	−0.22
Combined mooring/HYCOM-18.2	$\overline{T_c}$	−0.95	−0.28

The sign convention is positive northward and negative southward. A linear regression analysis for both the total transport and overflow transport showed no relationship between H and $M_o - M_H$, so $M_o - M_H$ was treated as a constant when calculating mean transports.

[a] Transport below 350 m.

[b] Omitted because the deep channel is so narrow there is no need for a model-based adjustment for cross-sectional velocity structure and $\overline{T_c}$ for the overflow was estimated from $M_o + (\overline{H} - H)$.

2008, plus large seasonal variability with seasonal transport reversals evident in all but 2004 (Figure 4d).

In addition to the estimate of total Mindoro Strait transport, separate estimates were made for the deep overflow clearly evident in Figure 4a–c. These estimates were defined as transports deeper than 350 m. Because the strait is narrow at these depths, no model-based adjustment for cross-sectional velocity structure was used. Table 3 gives the overflow transports based on the mooring data and 1/12° global HYCOM-18.2 for the observation period and 2004–2009. Table 2 gives the overflow transports for additional model experiments. At 0.28 Sv, the overflow contributes 29% of the estimated 2004–2009 mean southward transport through Mindoro Strait.

For comparison, Qu and Song (2009) found a "zero-order" estimate of 2.4 Sv for Mindoro Strait transport over the period 2004–2007, which they describe as providing "a useful upper bound of strait transport based solely on satellite observations." Yaremchuk et al. (2009) found a Mindoro Strait transport of 1.5 ± 0.4 Sv, using an inverse modeling approach. The transport was obtained from an optimized solution to a 4½ layer reduced-gravity model of the South China Sea that best fit the temperature, salinity, and mixed layer thickness of an ocean climatology. Estimates from relatively high resolution global ocean models include ~ 1.3 Sv from a 1/10° OfES simulation (Qu et al., 2006; Qu and Song, 2009) and 1.77 Sv from a 1/6° MOM2 simulation (Fang et al., 2005). All of the estimates are southward transports.

THE BOHOL SEA AND DIPOLOG STRAIT

The Bohol Sea inflow through the shallow Surigao Strait and outflow through Dipolog Strait form part of a second and shallower major pathway connecting the circulation within the Philippine Archipelago to the large-scale ocean circulation (Figure 1), but one that is deeper than the pathway feeding into the Indonesian Archipelago via the Karimata Strait connection to the Java Sea. As discussed earlier, the larger sill topography error in 1/25° global HYCOM-4.1&2 has less impact on the transport along this pathway. Dipolog Strait is the deepest of the five straits connecting to the Bohol Sea, but it is much shallower than the ~ 1500-m depth of the sea itself. The shallow surface jet and isolation of the deep basin result in a four-layer flow through the strait. The four-layer flow structure in Dipolog Strait was observed in PhilEx cruise conductivity, temperature, depth (CTD)/lowered ADCP surveys (Gordon et al., 2011) and in mooring velocity measurements made by J. Sprintall. It is also depicted in 1/25° global HYCOM-4.1&2, which has a weak lower overturning cell and a sill depth half that observed (Figure 5a, with a vertical line at the mooring location).

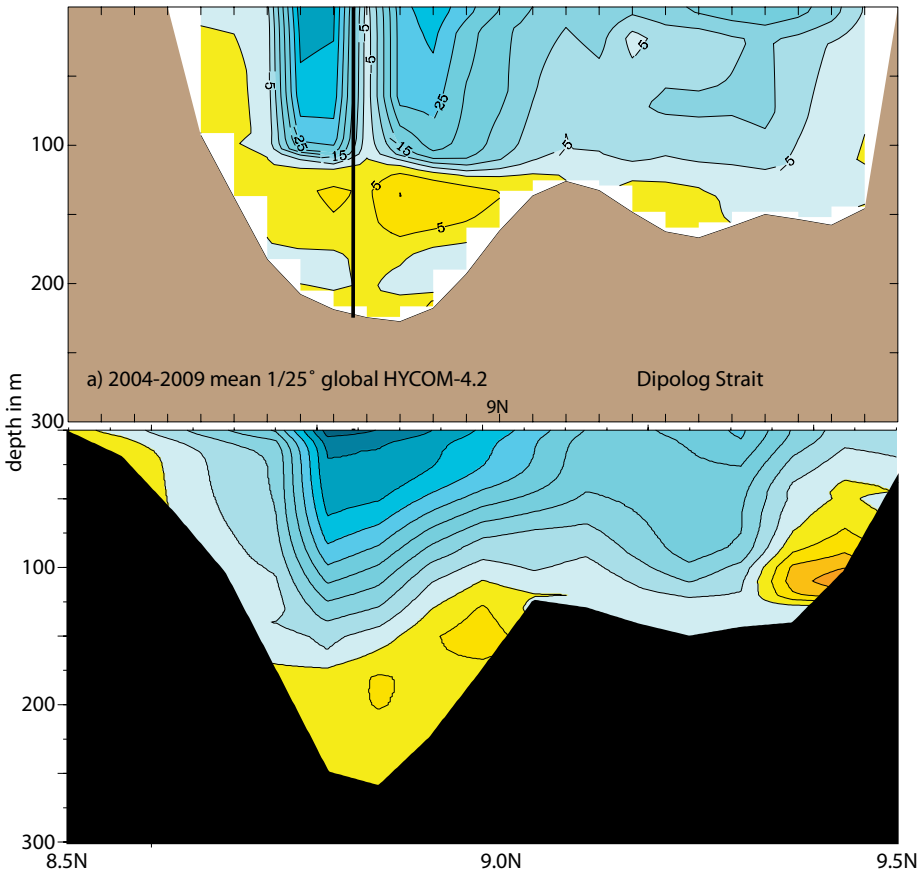

Figure 5. Dipolog Strait 2004–2009 mean zonal velocity cross sections at 123°22'E, the longitude of the PhilEx mooring (marked with a vertical line) that is located near the sill, from (a) 1/25° global HYCOM-4.2 and (b) EAS NCOM. Velocity has 0.05 m s^{-1} contour intervals with blue westward and yellow-red eastward.

The four-layer flow occurs because an inertial westward surface jet with strong vertical shear at its base entrains water from below that is fed by eastward flow from the Sulu Sea. The deeper overturning cell is driven by vertical mixing in the Bohol Sea, thought to be largely due to internal tides. Tides are not included in the simulation depicted in Figure 5a, although the K-Profile Parameterization (KPP) vertical mixing scheme of Large et al. (1994) contains a simple parameterization of the effects of internal wave breaking and vertical shear, and a contribution from tides is included in the parameterization of bottom friction. The vertical mixing reduces the Bohol Sea density below the sill depth and creates a pressure gradient that drives denser Sulu Sea water into the Bohol Sea just above the sill, which is compensated by the westward outflow just above (based on an explanation of the four-layer flow by Gordon et al., 2011). The 1/12° global HYCOM-18.2 does not have the shallow sill depth bias in Dipolog (Figure 1c), but it does not exhibit the deeper cell due to a thick model layer straddling the sill (not shown).

> "...THE PHILIPPINE ARCHIPELAGO POSES SEVERE TESTS FOR THE MODELS, TESTS THAT ARE PERFORMED USING DATA FROM THE PHILEX FIELD PROGRAM AND OTHER SOURCES."

The four-layer flow is not present in the Dipolog Strait section from EAS NCOM with tides (Figure 5b). EAS NCOM includes data assimilation (but not assimilation of PhilEx data), and it has a shallow bias in Dipolog sill depth similar to Figure 5a. While EAS NCOM has accurate temperatures at all depths in the Sulu Sea in comparison to unassimilated PhilEx CTD profiles, it has a cold deep bias of ~ 6°C in the Bohol Sea, making it colder than deep temperatures in the Sulu Sea and suggesting the possibility of westward bottom flow through Dipolog. Such flow is not seen in Figure 5b because the shallow Dipolog Strait sill in EAS NCOM is shallower than the deep temperature bias. The data assimilation projects surface data downward via synthetic temperature and salinity profiles based on statistics of the historical hydrographic data base (Fox et al., 2002). Due to a lack of Bohol Sea historical data, the Bohol Sea synthetics are contaminated by data from the Pacific and the Sulu Sea. The HYCOM simulations (Table 1) did not have data assimilation and were initialized from GDEM3 hydrographic climatology (Carnes, 2009), which has realistic deep temperatures in the Bohol Sea.

A small gap in the westward surface jet is evident near the mooring location in Dipolog Strait (Figure 5a). The mooring lies in the lee of a small rise capped by Silino Island, a feature not present in EAS NCOM. In HYCOM, the gap in the westward flow results in a large meridional gradient in the surface jet at the location of the mooring, making it difficult to use the model and mooring data to estimate Dipolog Strait transport, as was done at Mindoro Strait, even if the model sill depth error was corrected. Instead, hull-mounted ADCP measurements from a PhilEx cruise (Figure 6a) are compared with contemporaneous March 1–8, 2009 means from the three model experiments depicted in Figure 6: (b) 1/12° global HYCOM-18.2, (c) EAS NCOM, and (d) 1/25° global HYCOM-4.2. In each case, the current vectors are plotted at the resolution of the model. All of the models simulate the westward surface jet across the northern Bohol Sea with flow passing on both sides of Siquijor Island. At 21-m depth, the observed mean speed of this jet (black vectors in Figure 6a) is 0.56 m s^{-1} between the inflow from Surigao Strait near 125°24'E and the Dipolog Strait outflow near 123°E. Using the Figure 6 model currents at 20-m depth interpolated to the observation locations, a few of which lay outside the model jets, the model mean speeds and vector correlations with the observations are 0.32 m s^{-1} and 0.68 for 1/12° global HYCOM-18.2, 0.45 m s^{-1} and 0.80 for 1/25° global HYCOM-4.2, and 0.46 m s^{-1} and 0.76 for EAS NCOM. In the ADCP data, the jet is robustly evident at 81-m depth and weakly evident at 101 m, corroborating the sharp gradient in velocity at the base of the current simulated by 1/25° HYCOM-4.1&2

(Figure 5a), but at a slightly shallower depth in the observations. Similar results for the depth structure were obtained from other PhilEx cruises. Additionally, the ADCP observations corroborate the robust transport through Surigao Strait simulated by the models.

The hull-mounted ADCP measurements also depicted a robust cyclonic gyre in the western Bohol Sea during every PhilEx cruise. The mean speed of the measured gyre currents at 21-m depth was 0.34 m s^{-1} in June 2007, 0.26 m s^{-1} in December 2007, 0.25 m s^{-1} in January 2008, and 0.36 m s^{-1} in March 2009. Current vectors measured at 21-m depth during March 1–8, 2009, provide a striking depiction of this gyre adjacent to the main westward current through the Bohol Sea (Figure 6a). In Figure 6, only 1/25° HYCOM simulates a robust cyclonic gyre (0.36 m s^{-1} mean speed observed [red vectors in Figure 6a] versus 0.14 m s^{-1} and a vector correlation of 0.48 at corresponding locations in the model). At times, 1/25° HYCOM even simulates the small anticyclonic gyre observed south of Siquijor Island. EAS NCOM simulates an anticyclonic gyre in the Bohol Sea and 1/12° HYCOM-18.2 simulates no gyre, only coastal upwelling in the two southern bays (current vectors emanating from a boundary). Coastal upwelling and downwelling (current vectors terminating near a boundary) are evident in the other two simulations as well. A cyclonic gyre in the western Bohol Sea is present at 20-m depth in the six-year mean from 1/25° global HYCOM-4.1&2 (Figure 1b), but not at that depth in the mean from 1/12° global HYCOM-18.2 (Figure 1a), although it is present below ~ 50 m. In the ADCP measurements, this gyre extends to a depth of ~ 100 m versus ~ 120 m in 1/12° and 1/25° global HYCOM simulations.

Ocean color is also useful in evaluating the performance of ocean models, and, in turn, the models are useful in identifying ocean circulation features depicted in surface chlorophyll products (Chassignet et al., 2005; Shriver et al., 2007). Ocean color can depict both near-surface circulation features and areas of upwelling and downwelling. A persistent cyclonic gyre in the Bohol Sea is observed in ocean color (Cabrera et al., 2011) and in ADCP velocities, and it is simulated by models with sufficient resolution. In Figure 7, mean values of chlorophyll observed by the Moderate Resolution Imaging Spectroradiometer (MODIS) satellite (at 1-km resolution) in March 2007 (Figure 7a) are compared with March 2007 mean currents at 20-m depth from (b) 1/12° global

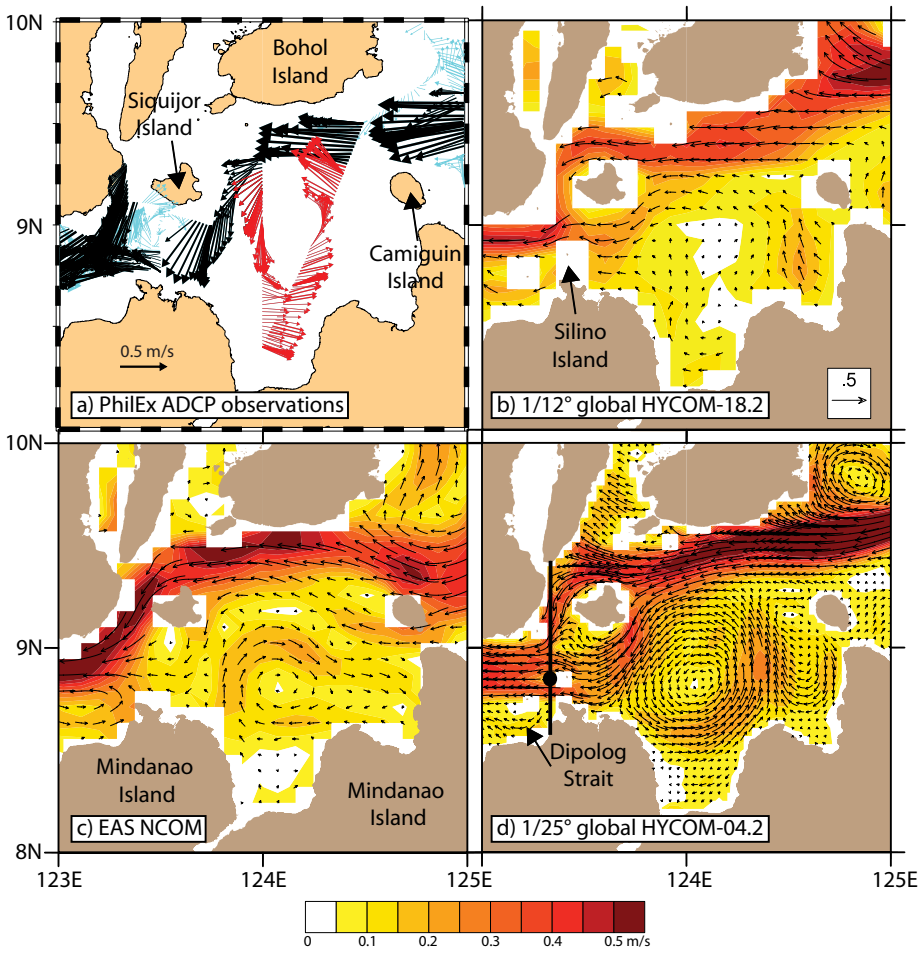

Figure 6. (a) ADCP velocity vectors at 21-m depth observed in the western Bohol Sea during March 1–8, 2009 versus March 1–8, 2009 mean currents at 20 m overlaid on speed from (b) 1/12° global HYCOM-18.2, (c) EAS NCOM, and (d) 1/25° global HYCOM-4.2. The reference vector for velocity is 0.5 m s^{-1} and mean speed is contoured at 0.05 m s^{-1} intervals. The black line in (d) defines the location of the cross section used in Figure 5, and the black dot denotes the mooring location. The observed mean speed of the westward jet (black vectors in panel a) is 0.56 m s^{-1}, and within the cyclonic gyre (red vectors) it is 0.36 m s^{-1}, both at 21 m depth. See text for model-data comparisons. To avoid a biased comparison, the observational result was chosen before the contemporaneous model results were extracted, a procedure also used for Figure 7.

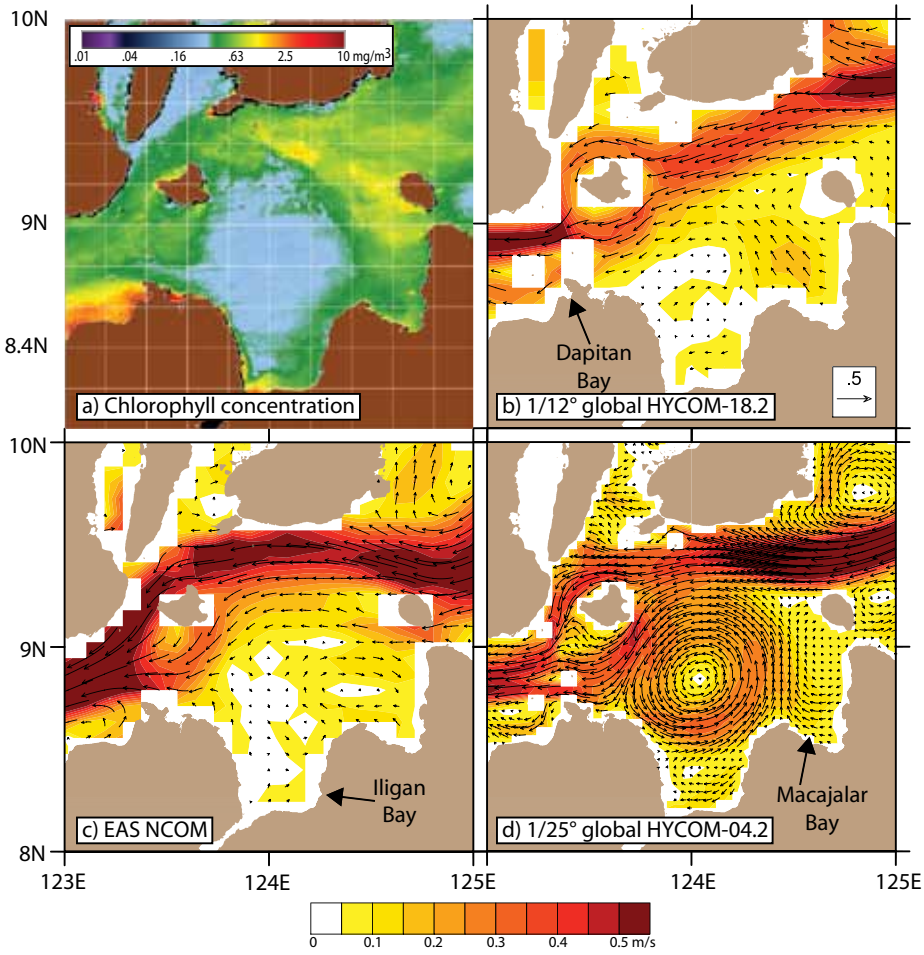

Figure 7. Same as Figure 6 but for March 2007 means, and panel (a) is replaced by chlorophyll concentration in mg m^{-3}.

HYCOM-18.2, (c) EAS NCOM, and (d) 1/25° global HYCOM-4.2. Chlorophyll concentrations characterize the cyclonic gyre as an oligotrophic center. Elevated concentrations occur along frontal boundaries and in upwelling centers at the southern boundaries. The results from the three models are similar to corresponding results in early March 2009 (Figure 6), but differ in detail. Again, all three models simulate the westward jet, depicted as a band of relatively high chlorophyll (Figure 7a). At the southern edge, the low-chlorophyll Bohol Sea gyre is marked by a zonal band of slightly elevated chlorophyll across Iligan Bay near 8.4°N. A narrow plume of low-chlorophyll water from the gyre enters the westward jet between Silino and Mindanao islands (see Figure 6 for locations). The position of the cyclonic gyre in 1/25° global HYCOM-4.2 is in close agreement with ocean color (Figure 7a,d), including a portion of the jet from the western edge of the gyre passing south of Silino Island, a jet also seen south of a gap in the five-year mean velocity cross section simulated by 1/25° HYCOM (Figure 5a). As in Figure 6, the other two models were not successful in depicting the cyclonic gyre (Figure 7b,c).

Parts of two small eddies are also indicated by low chlorophyll, one in the northeast corner, the other east of Camiguin Island. EAS NCOM and 1/25° HYCOM depict an anticyclonic eddy in the northeast corner and 1/25° HYCOM a cyclonic eddy east of Camiguin Island. In Iligan Bay, south of the main gyre, the chlorophyll is relatively high on the east side and low on the west side, except for very high chlorophyll at the mouth of an estuary in the southwestern corner. This pattern is consistent with coastal upwelling on the east side and downwelling to the west, as seen in the 1/12° and 1/25° global HYCOM simulations. Additionally, the ocean color indicates upwelling in Macajalar Bay, again seen in the two HYCOM simulations. In the ocean color, there is evidence of relatively strong upwelling on the west side of Camiguin Island and on both sides of the strait between Camiguin and Mindanao islands. The resulting high chlorophyll is advected to the northwest by a westward jet exiting through this strait, a feature depicted only in EAS NCOM (Figure 7c). A very narrow band of low chlorophyll is depicted along the southeastern coast of Bohol Island, consistent with the downwelling simulated by 1/25° HYCOM and seen to a lesser extent in EAS NCOM. Very high chlorophyll is seen in Dipolog Strait along the coast of Mindanao. It emanates from Dapitan Bay, possibly due to riverine outflow. This outflow plume is advected downstream by a westward coastal current that passes between the islands of Silino and Mindanao, a current depicted in 1/12° and 1/25° global HYCOM.

The 1/25° global HYCOM simulates a Bohol Sea cyclonic gyre in every

seasonal mean, most strongly in the winter mean (January–March), successively weaker in spring and fall, and only weakly in summer. The 1/12° HYCOM-18.2 simulated a mean cyclonic gyre every year during winter except 2009 (e.g., Figure 6b), every year during spring, but not during the last half of the year. During winter, EAS NCOM alternates between states with a cyclonic gyre, an anticyclonic gyre, and no gyre. Over 2004–2009, EAS NCOM simulated a realistic cyclonic gyre in only three seasonal means (~ 10 cm s^{-1} in spring 2006, 2008, and 2009) and one annual mean (~ 5 cm s^{-1} in 2008).

The westward jet along the northern boundary, its curvature to the southwest, and the basin depth (which reduces the impact of bottom friction) are conducive to generation of positive relative vorticity and formation of a cyclonic gyre within the western Bohol Sea. An additional mechanism, proposed by Cabrera et al. (2011), is based on the upwelling that occurs when the Bohol Sea subsurface inflow is entrained into the westward surface jet above (Figure 5). This upwelling stretches the water column, thus requiring cyclonic rotation in order to conserve potential vorticity. However, the conditions are not always sufficient for these mechanisms to work, as evidenced in Figures 6 and 7. What additional factors might be associated with the gyre formation and its variation in strength in the model simulations? The largest impact comes from doubling the model resolution from ~ 9 km to 4.4 km. Three other mechanisms are identified that clearly have an influence: (1) Dipolog Strait transport, which affects the strength of the mechanisms described above, (2) wind stress curl over the Bohol Sea, and (3) nondeterministic variability due to flow instabilities. A preconditioning impact from the previous season was not identified, nor was there any evidence of an independent impact from the latitude and angle of the surface jet entry into the western Bohol Sea north and south of Camiguin Island. Evidence of an impact is greatest for the strength of the Dipolog Strait transport. In 1/25° HYCOM-4.0, the seasonal variability in the strength of the Dipolog Strait transport and the strength of the Bohol Sea cyclonic gyre vary in tandem with the greatest strength in winter and successively weaker strength in spring, fall, and summer. In 1/12° HYCOM-18.2, the Bohol Sea cyclonic gyre is simulated only during the two seasons with the greatest Dipolog Strait transport, but those two seasons are reversed from 1/25° HYCOM-4.0 with the strength in spring greater than in winter for both transport and gyre strength. The mean wind stress curl in the Bohol Sea is positive in three seasons, strongest in winter and successively weaker in fall and spring, but it is negative in summer, an ordering different from that of the cyclonic gyre and Dipolog transport strength. However, the interannual variability of seasonal means in winter, the season with the strongest positive wind stress curl, did show a stronger gyre in the years with the strongest wind stress curl, independent of the relative jet strength. The climatologically forced simulations demonstrated nondeterministic variability in jet transport and gyre strength, and nondeterministic variability in gyre strength that at times was independent of jet transport. Such variability in gyre strength is also evident in interannual simulations.

The Regional Ocean Modeling System (ROMS) simulations of Han et al. (2009) have 5-km resolution, but depict the Bohol Sea gyre less robustly than 1/25° global HYCOM; for example, it is evident in their 2006 annual mean, but not in the means for 2004 and 2005, the other years depicted. It is also evident in June of 2006 and 2007, but is much weaker than observed in the January 2008 PhilEx ADCP data, and not evident in December 2005, January 2006, and August 2006, the other months depicted. In discussing the dynamics, the authors place greater emphasis on the impacts of Ekman transport and wind stress curl, which are less evident in the HYCOM simulations.

SIMULATION OF TIDES IN THE PHILIPPINE ARCHIPELAGO

The 1/12° HYCOM-14.1&2 is the first eddy-resolving global ocean simulation (e.g., one like 1/12° global HYCOM-18.2) that also includes external and internal tides (Arbic et al., 2010). As illustrated by the sunglint imagery in Figure 8a, internal tides can have a strong surface signature in the interior Philippine seas. Figure 8b shows a snapshot of the steric SSH anomaly with respect to a 25-hour mean from 1/12° global HYCOM-14.2, a month-long repeat of HYCOM-14.1 with global hourly three-dimensional output for May 2004. While not contemporaneous with the sunglint observation, HYCOM-14.2 has a clear representation of this surface signal that is generated in the same location and further indicates that internal tides are ubiquitous within the Philippine seas. Jackson et al. (2011) find internal waves observed by satellite imagery and Girton

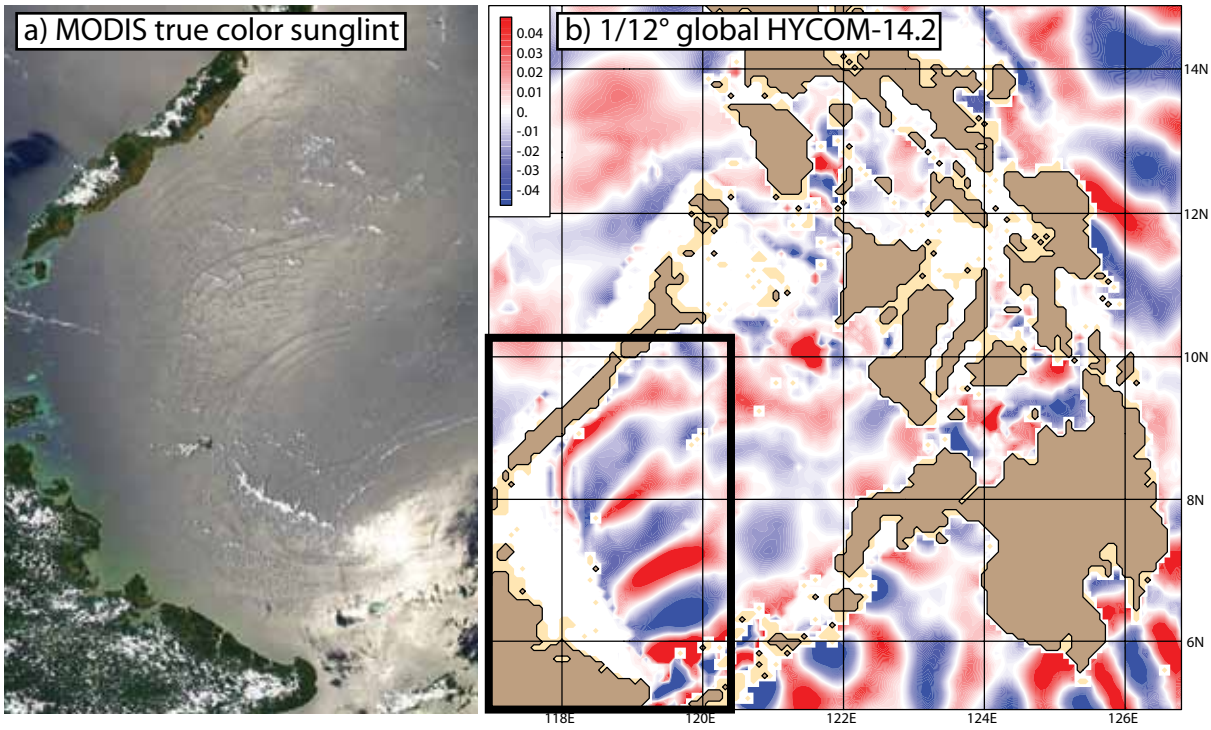

Figure 8. (a) Moderate Resolution Imaging Spectroradiometer (MODIS) true color sunglint image of the western Sulu Sea on April 8, 2003. Note the SSH signature of the internal tides that are generated in Sibutu Passage and propagate at speeds of ~ 2½ m s^{-1}. (b) Steric SSH anomaly (in m) from a 25-hour average centered on May 15, 2004, 12Z from 1/12° global HYCOM-14.2 with tidal forcing for the area in and around the Philippine seas. The black box outlines the region of the MODIS image. While not contemporaneous, global HYCOM has a similar SSH signature of the internal tides, but without the soliton packets, because solitons have nonhydrostatic physics and HYCOM is a hydrostatic model. Also note the strong internal tidal signatures in Mindoro Strait and the Bohol Sea, both focus areas for the PhilEx Intensive Observational Period cruises.

et al. (2011) by in situ data in several areas within the Philippine seas, and, like Apel et al. (1985), internal tidal beams, generated in Sibutu Passage, that propagate across the Sulu Sea (depicted in Figure 8a,b). In HYCOM-14.2 the maximum peak to peak amplitude of this internal tidal beam is 0.18 m in the steric SSH and ~ 40 m in the pycnocline after separation from Sibutu Passage. The propagation speed of the simulated internal tides (2.5 m s^{-1}) in the Sulu Sea is close to the observations of internal tides with similar amplitude (2.4 m s^{-1}; Apel et al., 1985). Because HYCOM is a hydrostatic model, it simulates only the hydrostatic physics of internal tides, not the nonhydrostatic physics required for simulation of the soliton packets generated by tidal cycles in the Sulu Sea (Apel et al., 1985) and visible in the sunglint imagery. Theoretical work by St. Laurent and Garrett (2002) suggests that tidal beams are primarily low vertical mode waves capable of propagating for distances of O(1000 km) with dissipation occurring due to critical slope interactions and bottom scattering. These mechanisms cause enhanced mixing, especially near the bottom. Tidal beams propagating > 1000 km occur in large ocean basins in HYCOM-14.1&2.

SUMMARY AND CONCLUSIONS

The circulation within the Philippine Archipelago is an integral component of the large-scale ocean circulation in a region of interbasin exchange. In that role, it provides two significant secondary routes for both the Indonesian throughflow and the western boundary currents that close the Pacific northern tropical gyre in addition to the Mindanao Current. The deeper route enters the archipelago from the north through Mindoro Strait, after passing through Luzon Strait and the South China Sea. The second route is very shallow and enters directly from the Pacific via Surigao Strait and

passes through Dipolog Strait downstream. Though shallow, the second route is deeper than the pathway entering the Indonesian Archipelago via Karimata Strait in the western Java Sea. Both routes through the Philippine Archipelago exit at the southern end via Sibutu Passage and the adjacent Sulu Archipelago. Within the Philippines, these secondary pathways are the dominant contribution to the mean circulation and much of its variability. In all of the 1/12° and 1/25° global HYCOM simulations the outflow from Sibutu Passage contributes to the southward flow through Makassar Strait at all depths above the Sibutu Passage sill, but despite their differences in Sibutu Passage transport, all simulate nearly the same transport through Makassar Strait, which carries the largest contribution to the Indonesian throughflow.

The 1/12° and 1/25° global HYCOM simulations and archived real-time data-assimilative nowcasts from EAS NCOM, nested in global NCOM, were used to study the circulation in the Philippine Archipelago within the context of global ocean circulation. However, because the straits are narrow and shallow and the interior seas are small, the simulations are very sensitive to model resolution and to the accuracy of the topography and sill depths within the narrow straits. In some cases this results in serious simulation errors, such as the transport of the Mindoro to Sibutu route in some simulations and the Bohol Sea circulation in all but the 1/25° model.

Precise topography and sill depths are required to accurately simulate the effects of hydraulic control and partitioning of the effects of hydraulic and geostrophic control on the flows through straits. Results from theory relating the pressure head and the transport through narrow choke points in Surigao and San Bernardino Straits were used to explain the much larger model transport through Surigao despite similar widths at a choke point, similar pressure heads, and shallow sill depths that did not explain the difference. The results show the transport at San Bernardino is constrained by the sill depth, but the transport through Surigao is not because the choke point at the outflow is deep and the upstream shallow inflow is broad. Instead, the transport and the pressure head are reconciled by using the thermocline depth in the Bohol Sea (the depth of the modeled Surigao outflow) and excluding the effect of bottom friction. The robust Surigao transport and the ~ 100-m depth structure of the westward Surigao-Dipolog surface-trapped jet are supported by the hull-mounted ADCP data collected at multiple locations along the jet during each of the four PhilEx cruise periods.

The global simulations demonstrate that 2004 and 2008, the latter the central year of the PhilEx observational program, were extreme opposite anomalous years, highlighted by anomalously strong southward flow through Mindoro in 2004 and mean northward flow in and above the thermocline during 2008. Associated opposite SSH anomalies in the western tropical Pacific were verified by satellite altimetry. The northern edge of both anomalies was located at the latitude of Luzon Strait and was characterized by gradients in SSH that fed into the South China Sea and downstream into the Philippine Archipelago via Mindoro Strait. The SSH anomalies had little effect on the transport of the Surigao-Dipolog route, which demonstrated strong seasonal variability but weak interannual variability. At Surigao, the SSH associated with the anomalies at each end of the strait varied in tandem, so the yearly mean pressure head remained nearly constant. Thus, the inflow through Mindoro Strait was found to be the primary external source of interannual variability in Philippine Archipelago circulation.

> “...THE MODELS ARE USED TO HELP INTERPRET THE DATA AND THEIR ABILITY TO MEASURE OBSERVED PHENOMENA, TO PLACE THE OBSERVATIONS WITHIN THE CONTEXT OF THE LARGER-SCALE CIRCULATION AND ITS TEMPORAL VARIABILITY, AND TO HELP UNDERSTAND THE DYNAMICS OF OBSERVED PHENOMENA.”

The December 22, 2007 to March 18,

2009 data from a single PhilEx mooring in Mindoro Strait in combination with HYCOM simulation results allow the first estimate of transport through Mindoro Strait using in situ data. The model helped extend the data across the strait and beyond the anomalous period of the observations, giving a mean transport of 0.24 Sv northward during the observation period and a mean of 0.95 Sv southward over 2004–2009, with the deep overflow contributing 0.28 Sv (29%) of this transport.

The 1/25° global HYCOM simulates the observed four-layer flow through Dipolog Strait. The upper cell is driven by entrainment into the westward Surigao-Dipolog surface jet, which has high vertical shear at the base, and the lower cell by vertical mixing in the Bohol Sea. All four of the PhilEx cruises observed a robust cyclonic gyre in the Bohol Sea using velocity measurements from a hull-mounted ADCP. This gyre is well-simulated in 1/25° HYCOM with 4.4-km resolution in comparison to the cruise current measurements and to ocean color imagery, but poorly simulated in the two models with ~ 9-km resolution. The 1/25° HYCOM is the first global ocean model with such fine horizontal resolution and more than a few layers in the vertical.

The Philippine Archipelago is a region with strong internal tides. The 1/12° HYCOM was used in the first eddy-resolving global ocean simulation with both atmospherically forced circulation and tides. The model demonstrated the ability to realistically simulate the hydrostatic aspect of internal tides within the Philippine Archipelago, including the strong tidal beam observed crossing the Sulu Sea, but not the associated soliton packets, which are nonhydrostatic.

A real-time data assimilative global ocean prediction system, based on 1/12° global HYCOM, has been running in real time or near-real time at the Naval Oceanographic Office since December 22, 2006 (Hurlburt et al., 2008; Metzger et al., 2008; Chassignet et al., 2009). Real-time and archived results are available at http://www.hycom.org. The HYCOM system was used to provide nowcasts, forecasts, and boundary conditions for some of the regional models and prediction systems run as part of PhilEx. A global ocean prediction system, based on 1/25° global HYCOM with tides, is planned for real-time operation starting in 2012. At this resolution, a global ocean prediction system can directly provide boundary conditions to nested relocatable models with ~ 1-km resolution anywhere in the world, a goal of US Navy operational ocean prediction. Knowledge gained in this study is being used to improve the performance of subsequent model simulations covering this region.

ACKNOWLEDGEMENTS

This work was sponsored by the Office of Naval Research under 6.1 program element 601153N, primarily via the Philippine Straits Dynamics Experiment (PhilEx), a 6.1 Directed Research Initiative, but also via the 6.1 projects "Dynamics of the Indonesian throughflow (ITF) and its remote impact" and "Global remote littoral forcing via deep water pathways" and by the 6.2 project "Full column mixing for numerical ocean models" (program element 602435N). The PhilEx DRI effort of J. Sprintall was supported by ONR Award N00014-06-1-0690. The computational effort was supported by the US Defense Department High Performance Computing Modernization Program via grants of challenge and non-challenge computer time. We thank PhilEx participant Chris Jackson for providing the MODIS sunglint image used in Figure 8. This is contribution NRL/JA/7304-10-419 and has been approved for public release.

REFERENCES

Apel, J.R., J.R. Holbrook, A.K. Liu, and J.J. Tsai. 1985. The Sulu Sea internal soliton experiment. *Journal of Physical Oceanography* 15:1,625–1,651.

Arango, H.G., J.C. Levin, E.N. Curchitser, B. Zhang, A.M. Moore, W. Han, A.L. Gordon, C.M. Lee, and J.B. Girton. 2011. Development of a hindcast/forecast model for the Philippine Archipelago. *Oceanography* 24(1):58–69.

Arbic, B.K., A.J. Wallcraft, and E.J. Metzger. 2010. Concurrent simulation of the eddying general circulation and tides in a global ocean model. *Ocean Modelling* 32:175–187.

Ashok, K., S.K. Behera, S.A. Rao, H. Weng, and T. Yamagata. 2007. El Niño Modoki and its possible teleconnection. *Journal of Geophysical Research* 112, C11007, doi:10.1029/2006JC003798.

Aviso (Archiving, Validation and Interpretation of Satellite Oceanographic data). 2010. DT CorSSH and DT SLA Product Handbook. CLS-DOS-NT-08.341, Edition 1.7. Available online at: http://www.aviso.oceanobs.com/fileadmin/documents/data/tools/hdbk_dt_corssh_dt_sla.pdf (accessed December 7, 2010).

Barron, C.N., A.B. Kara, P.J. Martin, R.C. Rhodes, and L.F. Smedstad. 2006. Formulation, implementation and examination of vertical coordinate choices in the global Navy Coastal Ocean Model (NCOM). *Ocean Modelling* 11(3–4):347–375.

Becker, J.J., D.T. Sandwell, W.H.F. Smith, J. Braud, B. Binder, J. Depner, D. Fabre, J. Factor, S. Ingalls, S.-H. Kim, and others. 2009. Global bathymetry and elevation data at 30 arc seconds resolution: SRTM30_PLUS. *Marine Geodesy* 32(4):355–371.

Bleck, R. 2002. An ocean general circulation model framed in hybrid isopycnic-Cartesian coordinates. *Ocean Modelling* 4:55–88.

Cabrera, O.C., C.L. Villanoy, L.T. David, and A.L. Gordon. 2011. Barrier layer control of entrainment and upwelling in the Bohol Sea, Philippines. *Oceanography* 24(1):130–141.

Carnes, M.R. 2009. Description and evaluation of GDEM-V3.0. NRL Memorandum Report NRL/MR/7330-09-9165. Naval Research Laboratory, Stennis Space Center, MS, USA. Available online at: http://www7320.nrlssc.navy.mil/pubs.php (accessed December 7, 2010).

Chassignet, E.P., L.T. Smith, G.R. Halliwell, and R. Bleck. 2003. North Atlantic simulation with the HYbrid Coordinate Ocean Model (HYCOM): Impact of the vertical coordinate choice, reference density, and thermobaricity. *Journal of Physical Oceanography* 33:2,504–2,526.

Chassignet, E.P., H.E. Hurlburt, O.M. Smedstad, C.N. Barron, D.S. Ko, R.C. Rhodes, J.F. Shriver, and A.J. Wallcraft. 2005. Assessment of ocean prediction systems in the Gulf of Mexico using ocean color. Pp. 87–100 in *Circulation in the Gulf of Mexico: Observations and Models*. Geophysical Monograph 161, W. Sturges and A. Lugo-Fernandez, eds, American Geophysical Union, Washington, DC.

Chassignet, E.P., H.E. Hurlburt, E.J. Metzger, O.M. Smedstad, J.A. Cummings, G.R. Halliwell, R. Bleck, R. Baraille, A.J. Wallcraft, C. Lozano, and others. 2009. US GODAE: Global ocean prediction with the HYbrid Coordinate Ocean Model (HYCOM). *Oceanography* 22(2):64–75. Available online at: http://www.tos.org/oceanography/issues/issue_archive/22_2.html (accessed December 29, 2010).

Fang, G., D. Susanto, I. Soesilo, Q. Zheng, F. Qiao, and Z. Wei. 2005. A note on the South China Sea shallow interocean circulation. *Advances in Atmospheric Sciences* 22(6):946–954.

Fang, G., R.D. Susanto, S. Wirasantosa, F. Qiao, A. Supangat, B. Fan, Z. Wei, B. Sulistiyo, and S. Li. 2010. Volume, heat and freshwater transports from the South China Sea to Indonesian seas in the boreal winter of 2007–2008. *Journal of Geophysical Research* 115, C12020, doi:10.1029/2010JC006225.

Fox, D.N., W.J. Teague, C.N. Barron, M.R. Carnes, and C.M. Lee. 2002. The Modular Ocean Data Analysis System (MODAS). *Journal of Atmospheric and Oceanic Technology* 19:240–252.

Girton, J.B., B.S. Chinn, and M.H. Alford. 2011. Internal wave climates of the Philippine seas. *Oceanography* 24(1):100–111.

Gordon, A.L., R.D. Susanto, A. Ffield, B.A. Huber, W. Pranowo, and S. Wirasantosa. 2008. Makassar Strait throughflow, 2004 to 2006. *Geophysical Research Letters* 35, L24605, doi:10.1029/2008GL036372.

Gordon, A.L., J. Sprintall, and A. Ffield. 2011. Regional oceanography of the Philippine Archipelago. *Oceanography* 24(1):14–27.

Han, W., A.M. Moore, J. Levin, B. Zhang, H.G. Arango, E. Curchitser, E. Di Lorenzo, A.L. Gordon, and J. Lin. 2009. Seasonal surface ocean circulation and dynamics in the Philippine Archipelago region during 2004–2008. *Dynamics of Atmospheres and Oceans* 47:114–137.

Hanley, D.E., M.A. Bourassa, J.J. O'Brien, S.R. Smith, and E.R. Spade. 2003. A quantitative evaluation of ENSO indices. *Journal of Climate* 16:1,249–1,258.

Hurlburt, H.E., E.P. Chassignet, J.A. Cummings, A.B. Kara, E.J. Metzger, J.F. Shriver, O.M. Smedstad, A.J. Wallcraft, and C.N. Barron. 2008. Eddy-resolving global ocean prediction. Pp. 353–381 in *Ocean Modeling in an Eddying Regime*. Geophysical Monograph 177, M. Hecht and H. Hasumi, eds, American Geophysical Union, Washington, DC.

Ilahude, A.G., and A.L. Gordon. 1996. Thermocline stratification within the Indonesian Seas. *Journal of Geophysical Research* 101(C5):12,401–12,409.

Jackson, C.R., Y. Arvelyna, and I. Asanuma. 2011. High-frequency nonlinear internal waves around the Philippines. *Oceanography* 24(1):90–99.

Kållberg, P., A. Simmons, S. Uppala, and M. Fuentes. 2004. ERA-40 Project Report Series: 17. The ERA-40 archive. ECMWF, Reading, Berkshire, UK, 31 pp. Available online at: http://www.mad.zmaw.de/uploads/media/e40Archive.pdf (accessed December 7, 2010).

Kara, A.B., A.J. Wallcraft, P.J. Martin, and R.L. Pauley. 2009. Optimizing surface winds using QuikSCAT measurements in the Mediterranean Sea during 2000–2006. *Journal of Marine Systems* 78:119–131.

Large, W.G., J.C. McWilliams, and S.C. Doney. 1994. Oceanic vertical mixing: A review and a model with a nonlocal boundary layer parameterization. *Reviews of Geophysics* 32(4):363–403.

Lermusiaux, P.F.J., P.J. Haley Jr., W.G. Leslie, A. Agarwal, O.G. Logutov, and L.J. Burton. 2011. Multiscale physical and biological dynamics in the Philippine Archipelago: Predictions and processes. *Oceanography* 24(1):70–89.

Mattsson, J. 1995. Observed linear flow resistance in the Öresund due to rotation. *Journal of Geophysical Research* 100:20,779–20,791.

Metzger, E.J., and H.E. Hurlburt. 1996. Coupled dynamics of the South China Sea, the Sulu Sea, and the Pacific Ocean. *Journal of Geophysical Research* 101(C5):12,331–12,352.

Metzger, E.J., H.E. Hurlburt, A.J. Wallcraft, J.F. Shriver, L.F. Smedstad, O.M. Smedstad, P. Thoppil, and D.S. Franklin. 2008. *Validation Test Report for the Global Ocean Prediction System V3.0 – 1/12° HYCOM/NCODA: Phase I.* NRL Memorandum Report NRL/MR/7320--08-9148. Naval Research Laboratory, Stennis Space Center, MS, USA. Available online at: http://www7320.nrlssc.navy.mil/pubs.php (accessed December 7, 2010).

Metzger, E.J., H.E. Hurlburt, X. Xu, J.F. Shriver, A.L. Gordon, J. Sprintall, R.D. Susanto, and H.M. van Aken. 2010. Simulated and observed circulation in the Indonesian Seas: 1/12° global HYCOM and the INSTANT observations. *Dynamics of Atmospheres and Oceans* 50:275–300, doi:10.1016/j.dynatmoce.2010.04.002.

Qu, T. 2000. Upper-layer circulation in the South China Sea. *Journal of Physical Oceanography* 30:1,450–1,460.

Qu, T., and Y.T. Song. 2009. Mindoro Strait and Sibutu Passage transports estimated from satellite data. *Geophysical Research Letters* 36, L09601, doi:10.1029/2009GL037314.

Qu, T., Y. Du, and H. Sasaki. 2006. South China Sea throughflow: A heat and freshwater conveyer. *Geophysical Research Letters* 33, L23617, doi:10.1029/2006GL028350.

Rosmond, T.E., J. Teixeira, M. Peng, T.F. Hogan, and R. Pauley. 2002. Navy Operational Global Atmospheric Prediction System: Forcing for ocean models. *Oceanography* 15(1):99–108. Available online at: http://www.tos.org/oceanography/issues/issue_archive/15_1.html (accessed December 29, 2010).

Shriver, J.F., H.E. Hurlburt, O.M. Smedstad, A.J. Wallcraft, and R.C. Rhodes. 2007. 1/32° real-time global ocean prediction and value added over 1/16° resolution. *Journal of Marine Systems* 65:3–26.

St. Laurent, L., and C. Garrett. 2002. The role of internal tides in mixing the deep ocean. *Journal of Physical Oceanography* 32:2,882–2,899.

Wang, Y.H., S. Jan, and D.P. Wang. 2003. Transports and tidal current estimates in the Taiwan Strait from shipboard ADCP observations (1999–2001). *Estuarine Coastal and Shelf Science* 57:193-199.

Yaremchuk, M., J. McCreary Jr., Z. Yu, and R. Furue. 2009. The South China Sea throughflow retrieved from climatological data. *Journal of Physical Oceanography* 39:753–767, doi:10.1175/2008JPO3955.1.